Ore Geology Reviews 112 (2019) 103037

Contents lists available at ScienceDirect

Ore Geology Reviews

journal homepage: www.elsevier.com/locate/oregeorev

Framboidal chalcopyrite and bornite constrain redox conditions during formation of their host rocks in the copper stratabound mineralization of Picachos, north-central Chile

R. Merinero[a,*], L. Ortega[a], R. Lunar[a], R. Piña[a], V. Cárdenes[b]

[a] Mineralogy and Petrology Department, Complutense University of Madrid, Avda. Complutense s/n, 28040 Madrid, Spain
[b] Geology Department, Oviedo University, C/Jesús Arias de Velasco s/n, 33005 Oviedo, Asturias, Spain

ARTICLE INFO

Keywords:
Framboidal pyrite
Framboidal chalcopyrite
Framboidal bornite
Representative size distributions

ABSTRACT

The Picachos Project is a copper deposit that occurs in manto-type orebodies in north-central Chile and it exhibits common features of Chilean stratabound or manto-type copper deposits: (1) an increase of copper contents from the margins to the centre of the orebodies; (2) sodic and potassic hydrothermal alteration of host rocks with subsequent chloritization and sericite alteration; and (3) its occurrence in sequences of limestones that are intercalated with volcanic rocks. The most salient characteristic of the Picachos Project is the presence of pervasive framboidal pyrite in both the non-mineralized limestones and the host rocks of the copper mineralization. These framboidal pyrites are well preserved, probably due to their close relationship with organic matter, and have no evident textures of overgrowth, recrystallization or dissolution. Moreover, framboidal chalcopyrite and bornite are formed in the external and internal areas, respectively, of the orebodies, sharing common morphological characteristics with framboidal pyrite, and are formed by the replacement of the original pyrite framboids, without changing their shape and size distribution. Representative size distributions of framboidal pyrite, chalcopyrite and bornite are determined using high-resolution X-ray tomography (micro-CT). This study highlights the effectiveness of these analytical techniques to obtain the representative size distribution of framboids in mineralized rocks. The preservation of the original framboidal texture of pyrite makes it possible to infer anoxic to near-dysoxic conditions. The size distributions of framboidal chalcopyrite and bornite are hypothesized to be additional potential paleo-redox indicators, referring to the same formation dynamic as typical framboidal pyrites.

1. Introduction

Framboids are the most common morphology of pyrite in sedimentary environments (Wilkin et al., 1996; Peckmann and Thiel, 2004; Schoonen, 2004; Cavalazzi et al., 2014). This morphology consists of a compact arrangement of microcrystals forming spherical shapes that resemble raspberries. The frequent presence in sedimentary environments of organic matter and simple alkane hydrocarbons, such as methane, favours the pyrite or precursor monosulphide supersaturation conditions that drive the formation of the multiple small microcrystals that form framboids (Wilkin and Barnes, 1997; Butler and Rickard, 2000).

The size distribution of framboidal pyrite can be used to constrain the paleo-redox formation environments of the rocks containing framboidal pyrite (Wilkin et al., 1996; Wignall and Newton, 1998; Bond and Wignall, 2010; Rickard, 2019). Differences in the mean and standard deviation of the sizes were observed by Wilkin et al. (1996) as a proxy of the sedimentary conditions. The determination of the size distribution of framboidal pyrite is mainly achieved by 2D techniques. However, there are many difficulties involved in translating these observations into their real distribution, among them the use of the diameter of circular sections to infer the real diameter of the framboids (e.g. Wignall and Newton, 1998; Wang et al., 2012; Tian et al., 2014; Xiao et al., 2018). Recently, 3D techniques like micro-CT have been used to solve these problems, obtaining near-real size distributions (Cárdenes et al., 2015, 2016, 2018; Merinero et al., 2017).

Framboidal pyrite can also form during diagenesis, such as in low-grade metamorphism and hydrothermal alteration (Scott et al., 2009). It often occurs in numerous sedimentary rocks affected by hydrothermal alteration, for example in volcano-sedimentary sequences associated with stratabound copper deposits (Hayes et al., 2015). In these rocks, framboidal pyrite rarely presents its original shape, because

* Corresponding author.
E-mail address: rmeriner@ucm.es (R. Merinero).

https://doi.org/10.1016/j.oregeorev.2019.103037
Received 3 April 2019; Received in revised form 18 July 2019; Accepted 26 July 2019
Available online 27 July 2019

hydrothermal alteration promotes the overgrowth, recrystallization, mineralogical transformation or dissolution of the framboids (e.g. Wilson and Zentilli, 1999; Cavalazzi et al., 2012; Carrillo-Rosúa et al., 2014; Sadati et al., 2016; Rajabpour et al., 2017). Therefore, the use of the size distribution of framboidal pyrite as a paleo-redox indicator is very limited in rocks with such hydrothermal alteration.

In this paper, we present a detailed mineralogical and geochemical study of the stratabound copper type mineralization at the Picachos Project (north-central Chile), where framboidal pyrite occurs pervasively in the limestone host rocks. Original framboidal pyrite is well preserved in the mineralized limestones, and the size distribution representing paleo-redox conditions could be determined using micro-CT, coupled with previously used filtering methods (Merinero et al., 2017). Moreover, since framboids of chalcopyrite and bornite have preserved the original framboidal texture of the pyrite, the paleo-redox conditions of limestone formation could also be determined from the size distribution of these minerals.

2. Regional context of the Picachos copper Project

The Picachos Copper Project, operated by Herencia Resources Plc, covers 410 ha and is located at an approximate elevation of 800 m above sea level in the Coastal Range of north-central Chile. Geographically, it occurs to the south of the Elqui Province, Coquimbo Region, Chile, approximately at 292 700 E and 6 649 100 N. It is situated about 350 km northeast of Santiago, 42 km southeast of La Serena city, 8 km southwest of the large Andacollo gold-copper deposit (Reyes, 1991; Guzmán et al., 2000), and 10 km south of the small Tambillos copper mine (Fig. 1).

The Coastal Range of north and north-central Chile comprises thick Jurassic and Lower Cretaceous volcano-sedimentary formations generated in extensional back-arc basins and an active convergent margin, respectively. These volcano-sedimentary formations are intruded by Lower to Upper Cretaceous calc-alkaline granitoids (diorites to granodiorites and tonalites) and overprinted by very low-grade regional metamorphism and hydrothermal alteration (Pichowiak, 1994; Dallmeyer et al., 1996; Oliveros et al., 2006). The main assemblage of this low-grade hydrothermal alteration is chlorite-epidote-quartz-calcite-titanite-sericite-actinolite-K-feldspar-zeolite-prehnite-pumpellyite (Oliveros et al., 2006).

In the vicinity of the Picachos Project, volcano-sedimentary formations are represented by the Arqueros and Quebrada Marquesa formations. The Arqueros Formation was deposited in a littoral environment under shallow-marine conditions, and comprises lava flows with intercalations of shallow limestones (Aguirre and Egert, 1965; Emparán and Pineda, 2006). The Quebrada Marquesa formation is mainly composed of tuffs and tuff-breccias with minor marine intercalations, continental volcanoclastic rocks and andesitic lavas (Aguirre and Egert, 1965; Emparán and Pineda, 2006).

The Picachos Project comprises numerous small copper mines and work sites covered by three concessions (Ermita, Los Ranchos and Prodiga), along with several prospects including 410 ha (Fig. 1). The Project's recent production consists mostly of small-scale mining. The copper mineralization occurs in stratabound manto-type bodies and mineralized veins cutting both the host rocks and the copper mantos. The mineralization is enriched along NW-SE feeder-faults, and within marine organic-rich limestones and calcareous sandstones. The thickness of the mineralized mantos, which is closely associated with subparallel NW-SE faults, is variable and ranges between 10 and 40 m. The continuity of the copper mantos can be traced over distances of up to 2 km. The mineral resources are estimated at approximately > 25 Mt, with grading at 1.0–1.2% Cu and 25 g/t Ag, respectively (2017, https://herenciaresources.com/our-operations/pastizal-picachos/).

3. Analytical methods

In order to carry out textural, mineralogical and geochemical studies, representative samples were selected from six exploration drill cores from Herencia Resources Plc, and from exposed surface outcrops. Detailed logging of > 40 m of three drill holes was performed in order to establish vein mineral relationships and textures. A total of 41 polished thin sections, including representative host rocks and vein mineralogy, were prepared and studied by transmitted and reflected light optical microscope.

3.1. Microprobe and SEM analysis

Ore mineral compositions were determined by electron microprobe in 12 samples using a JEOL Superprobe JXA-8900 at the Complutense University of Madrid's Centro Nacional de Microscopía Electrónica.

During compositional analyses, Kα X-ray lines were measured for S, As, Fe, Co, Ni, Cu, Zn and Pb. The accelerating voltage was 20 kV, with a 50 nA beam current and a beam diameter of 1–5 μm. Counting times ranged from 20 to 60 s. The following standards were used: Galena, GaAs, Fe, NiCrCo, Cu and Zn from the Smithsonian Institution and Harvard University (Jarosewich et al., 1980; McGuire et al., 1992).

3.2. High resolution X-ray computed tomography (micro-CT) analysis

Micro-CT was used in order to estimate the size distribution of framboidal minerals in five selected samples containing exclusively individual framboids (Fig. 2). We obtained cylindrical samples measuring 4 mm in diameter and 10 mm in length from each sample in selected zones with abundant framboidal minerals. These cylindrical samples were scanned with a tomographic system (Phoenix V|Tome|X S 240, GE) housed at the National Centre for the Research of Human Evolution, CENIEH (Burgos), using the following settings: nanofocus X-ray tube, voltage of 80 kV, amperage of 325 μA and exposure time of 2000 ms. > 1400 projections were obtained for each sample during a complete rotation along a vertical axis, achieving a voxel size of 1.6 μm. These projections were reconstructed using the program Amira (Visage Imaging). The reconstructed images were analysed following the four-step method of Merinero et al. (2017) and segmented 3D objects representing spherical objects were obtained using Fiji ImageJ distribution 1.52i (Schindelin et al., 2012) and the plugin Roi Manager 3D v3.92 (Ollion et al., 2013).

3.3. Statistical analyses

Data management and analyses were performed using the R v. 3.4.3 statistical software (R_Core_Team, 2017). The lognormality of the size populations obtained from the SEM analysis was assessed by quantile-quantile plots (QQ-plots) and applying the Shapiro-Wilk test of normality (Royston, 1995) to the natural logarithm of the size. The mixture of lognormal populations was analysed through the spherical 3D objects obtained from the micro-CT analysis and the four-step filtering process. The Mclust function of the R package mclust v. 5.4.1 (Scrucca et al., 2016) was used in order to estimate the optimal mixture model of lognormal populations by using hierarchical clustering.

4. Results

4.1. Copper mineralization at the Picachos Project

Copper mineralization at the Picachos Project is hosted by limestones of the Arqueros Formation (arenaceous and organic material-bearing limestones) intercalated with dacitic volcanic rocks. The hydrothermal alteration of volcanic rocks consists of extensive sodic and potassic alteration with subsequent chloritization and sericite alteration. Plagioclase is partially argillized and replaced by secondary K-

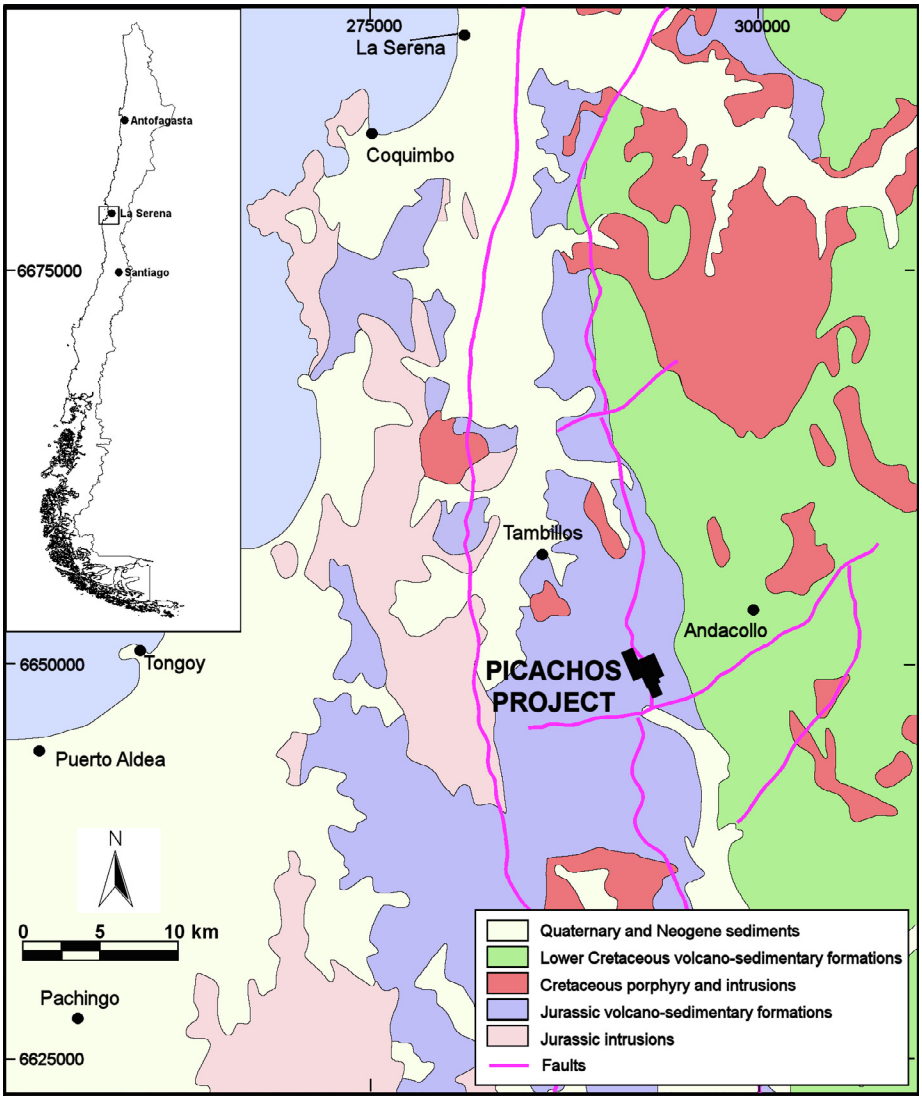

Fig. 1. Simplified regional geology of the Picachos Project in north-central Chile (inset).

feldspar and albite, and subsequently altered to chlorite, calcite and sericite. Primary K-feldspar is altered to kaolinite and sericite. Hornblende is partially replaced by secondary biotite, chlorite and opaque minerals such as magnetite and hematite. Primary biotite is replaced by chlorite and hematite along its margins.

Non-mineralized limestones mainly consist of calcite and pervasive pyrite forming framboids. Framboidal pyrite occurs in close relationship with preserved organic matter and euhedral ankerite (Fig. 3a and

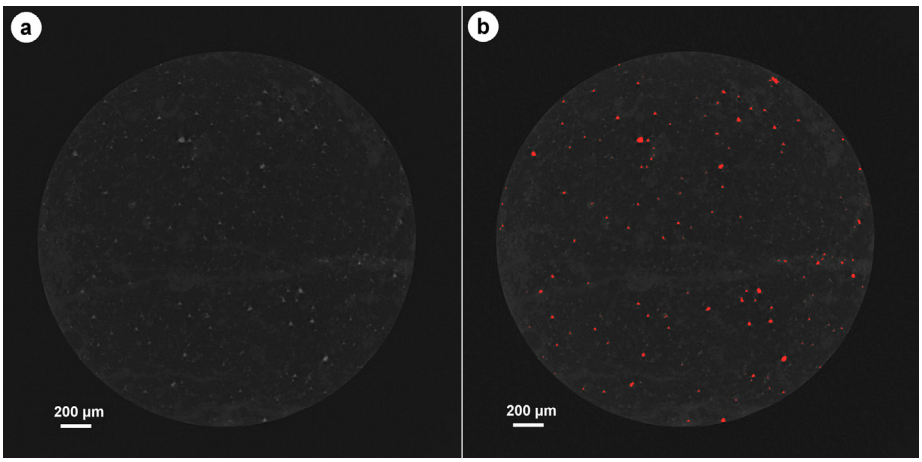

Fig. 2. (a) Representative micro-CT image showing individual framboids; (b) the same micro-CT image after apply thresholds in order to segment objects and measure diameters.

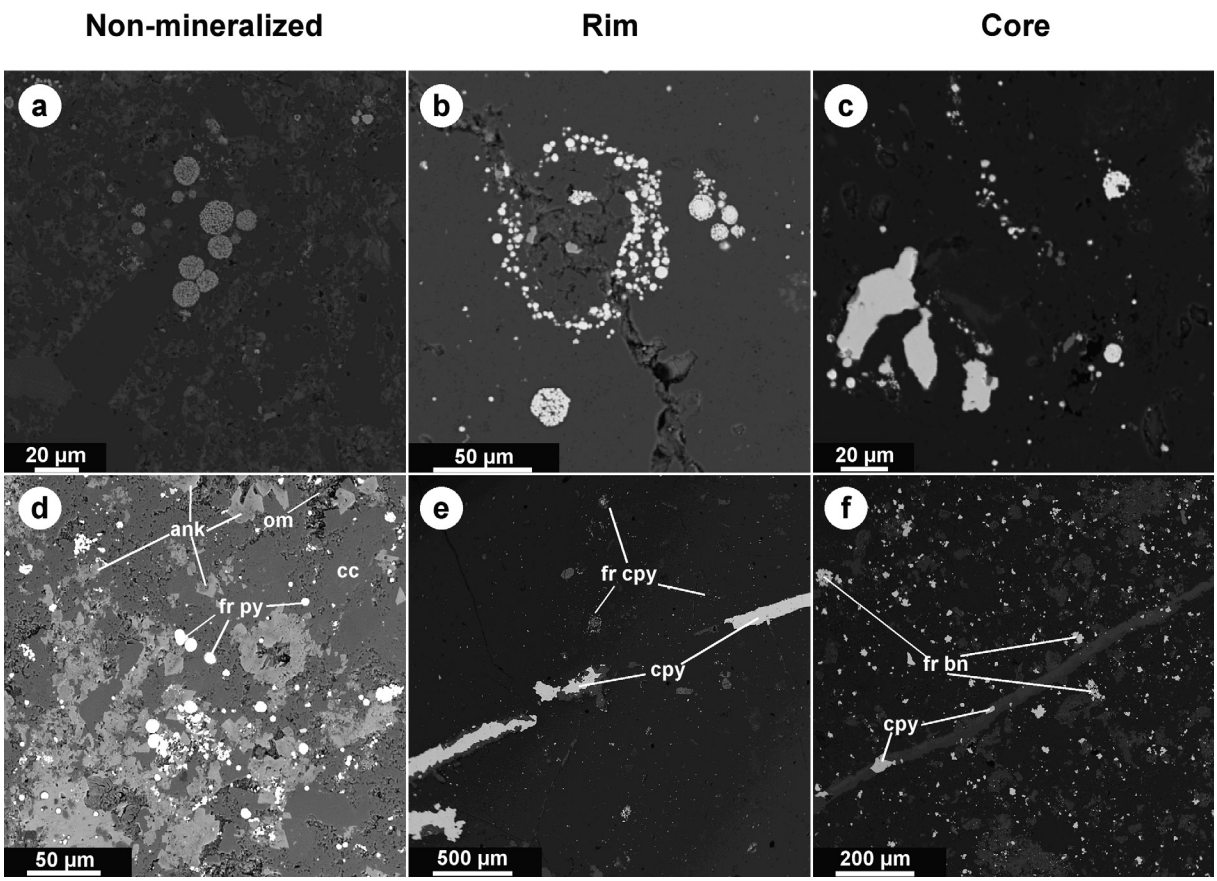

Fig. 3. Thin-section back-scatter SEM photomicrographs showing framboidal textures in non-mineralized limestones (a, d) at the margin (b, e) and the centre (c, f) of the orebodies. ank = ankerite; cc = calcite; cpy = chalcopyrite; fr bn = framboidal bornite; fr cpy = framboidal chalcopyrite; fr py = framboidal pyrite; om = organic matter.

d).

Mineralized bodies show a zoning of their copper content with iron-rich sulphides at their margins, and copper-rich sulphides at their central parts. The typical zoning of the orebodies in non-oxidized areas consists of chalcopyrite-(galena)-bornite-(chalcocite) assemblages in their central parts, and pyrite-(pyrrhotite) at their margins (Fig. 4). Representative microprobe analyses of pyrite, chalcopyrite and bornite are included in Table 1. Oxidized areas are characterized by the formation of supergene sulphides (chalcocite, digenite and covellite), copper carbonates (malachite and azurite), copper sulphates (chalcanthite and brochantite) and supergene iron oxides (hematites), respectively.

Massive pyrite is abundant at the margins of the zoned orebodies of the Picachos Project (Fig. 4d). In limestone-hosted mineralization, pyrite occurs with framboidal textures, forming disseminated framboids and, more rarely, small polyframboids. No overgrowths or sunflower textures are observed in the framboidal pyrite. Framboidal pyrite coexists with framboidal chalcopyrite at the margins of the mineralization, and it also coexists with framboidal bornite at the centre of the orebodies. Neither recrystallization (loss of internal texture), nor dissolution (loss of sphericity by the formation of holes) has been documented in the framboids. Massive pyrite exhibits Fe contents varying from 46.33 to 46.98 wt% and S contents varying from 51.95 to 52.64 wt %. The concentration of trace elements (Cu, Zn, As, Pb, Ni and Co) is generally < 100 ppm. The Fe and S contents in framboidal pyrite exhibit a greater variation than that of massive pyrite (see Table 1), ranging from 43.58 to 45.70 wt% for Fe and 51.61 to 53.46 wt% for S. The Cu, Zn, As, Ni and Co contents of framboidal pyrite are below the detection limit. However, the Pb content is higher and varies from 2100 to 9700 ppm.

Chalcopyrite is the most abundant copper sulphide in the Picachos Project and usually occurs as massive textures. In some places, chalcopyrite grains contain small inclusions of sphalerite and galena (Fig. 4a). Chalcopyrite replaces or is replaced by pyrite along the margins (Fig. 4d) and can be replaced by bornite and chalcocite in central parts of the orebodies (Fig. 4b and e). At the margins, chalcopyrite also occurs as individual framboids, and more rarely, as small clusters of framboids or polyframboids (Fig. 3b and e). Framboidal chalcopyrite does not represent overgrowth, recrystallization or dissolution textures. The Fe content in massive chalcopyrite varies from 29.60 to 30.22 wt%, the S content from 34.98 to 35.79 wt%, and the Cu content from 33.13 to 33.68 wt%. The trace element (Zn, As, Pb, Ni and Co) concentrations are < 100 ppm. By contrast, the framboidal chalcopyrite exhibit Fe and Cu contents with a higher range of variation: 26 to 40 wt% and 8.6 to 24.8 wt%, respectively (see Table 1). Framboidal chalcopyrite also contains appreciable amounts of Pb of up to 3300 ppm.

Bornite only occurs in the centre of the orebodies, where it usually either replaces chalcopyrite, or occurs as inclusions in massive chalcopyrite (Fig. 4b and e). In these places, bornite also occurs as disseminated framboids in the limestones that host mineralization. Framboidal bornite does not represent overgrowth, recrystallization or dissolution textures (Fig. 3c and f). The Fe content in massive bornite varies from 9.78 to 10.4 wt%, the S content from 25.9 to 26.5 wt%, and the Cu content from 60.9 to 63.7 wt% (see Table 1). The Zn, As, Pb, Ni and Co contents are < 100 ppm. Framboidal and massive bornite have a low range of variation in Fe and Cu contents: 9.8 to 10.8 wt% and 60.6 to 63.1 wt%, respectively (see Table 1). Framboidal bornite also contains appreciable amounts of Pb, of up to 1900 ppm.

The vein-type mineralization consists of mineralized veins and

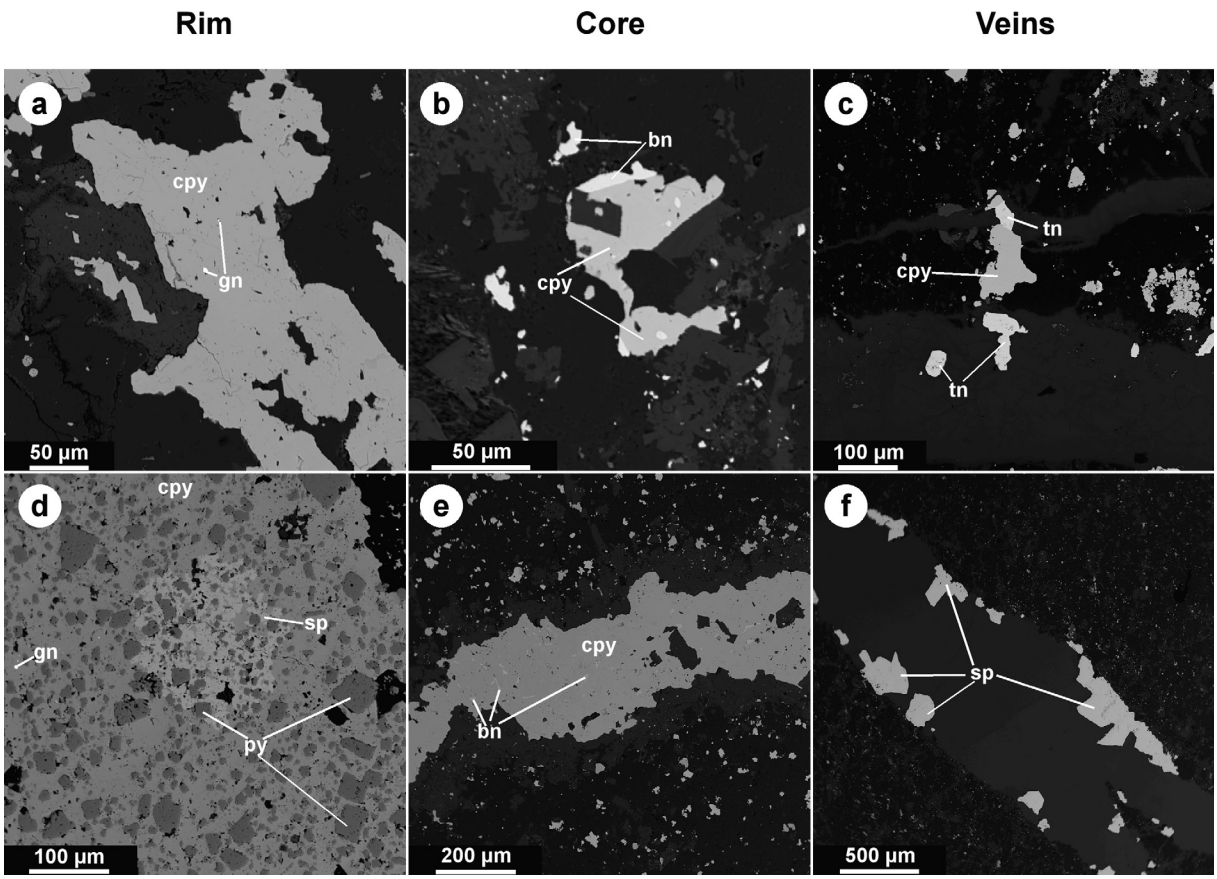

Fig. 4. Thin-section back-scatter SEM photomicrographs showing sulphide assemblages at the margin (a, d) and the centre (b, e) of the orebodies, and in the mineralized veins (c, f). bn = bornite; cpy = chalcopyrite; gn = galena; py = pyrite; sp = sphalerite; tn = tennantite.

veinlets of calcite intersecting the mantos-style copper mineralization. The mineralized veins and veinlets contain sphalerite, chalcopyrite and tennantite assemblages (Fig. 4c and f) and represent late stages of the mineralization.

4.2. Size distribution of framboidal textures

Five selected samples containing framboidal textures were analysed using micro-CT techniques. The representative size distribution of framboids in each sample was obtained from the analysis of the log-normal populations in the micro-CT.

Table 1
Representative microprobe analyses of massive and framboidal pyrite, chalcopyrite and bornite from mineralized and non-mineralized limestones of the Picachos Project (wt.% and calculated cations).

		Pyrite				Chalcopyrite				Bornite			
	d.l.	Massive		Framboidal Pn		Massive		Framboidal		Massive		Framboidal	
S	0.04	51.95	51.85	53.46	52.86	34.98	35.01	39.33	49.80	25.99	26.25	26.47	27.36
Fe^{2+}	0.02	46.44	46.98	43.59	45.69	30.11	30.23	29.33	39.99	9.79	10.38	9.93	10.78
Cu	0.04	*b.d.l.*	*b.d.l.*	*b.d.l.*	*b.d.l.*	33.65	33.92	30.63	12.82	63.71	60.92	63.10	60.92
As	0.02	*b.d.l.*	*b.d.l.*	*b.d.l.*	*b.d.l.*	*b.d.l.*	*b.d.l.*	*b.d.l.*	*b.d.l.*	*b.d.l.*	*b.d.l.*	*b.d.l.*	*b.d.l.*
Ni	0.02	*b.d.l.*	*b.d.l.*	*b.d.l.*	*b.d.l.*	*b.d.l.*	*b.d.l.*	*b.d.l.*	*b.d.l.*	*b.d.l.*	*b.d.l.*	*b.d.l.*	*b.d.l.*
Co	0.02	*b.d.l.*	*b.d.l.*	*b.d.l.*	*b.d.l.*	*b.d.l.*	*b.d.l.*	*b.d.l.*	*b.d.l.*	*b.d.l.*	*b.d.l.*	*b.d.l.*	*b.d.l.*
Pb	0.04	*b.d.l.*	*b.d.l.*	0.34	0.30	*b.d.l.*	*b.d.l.*	0.31	0.17	*b.d.l.*	*b.d.l.*	0.11	0.15
Zn	0.03	*b.d.l.*	*b.d.l.*	*b.d.l.*	*b.d.l.*	*b.d.l.*	*b.d.l.*	*b.d.l.*	*b.d.l.*	*b.d.l.*	*b.d.l.*	*b.d.l.*	*b.d.l.*
Total		99.08	99.61	97.53	99.11	98.99	99.26	99.68	98.69	99.54	97.68	99.66	99.27
S		1.99	1.97	2.04	2.00	2.02	2.01	2.19	2.58	4.08	4.17	4.13	4.25
Fe^{2+}		1.01	1.02	0.96	0.99	1.00	1.00	0.94	1.19	0.88	0.95	0.89	0.96
Cu		–	–	–	–	0.98	0.99	0.86	0.23	5.04	4.88	4.97	4.78
As		–	–	–	–	–	–	–	–	–	–	–	–
Ni		–	–	–	–	–	–	–	–	–	–	–	–
Co		–	–	–	–	–	–	–	–	–	–	–	–
Pb		–	–	–	–	–	–	–	–	–	–	–	–
Zn		–	–	–	–	–	–	–	–	–	–	–	–
Total		3.00	2.99	3.00	2.99	4.00	4.00	3.99	4.00	10.00	10.00	9.99	9.99

d.l. = detection limit; *b.d.l.* = below detection limit.

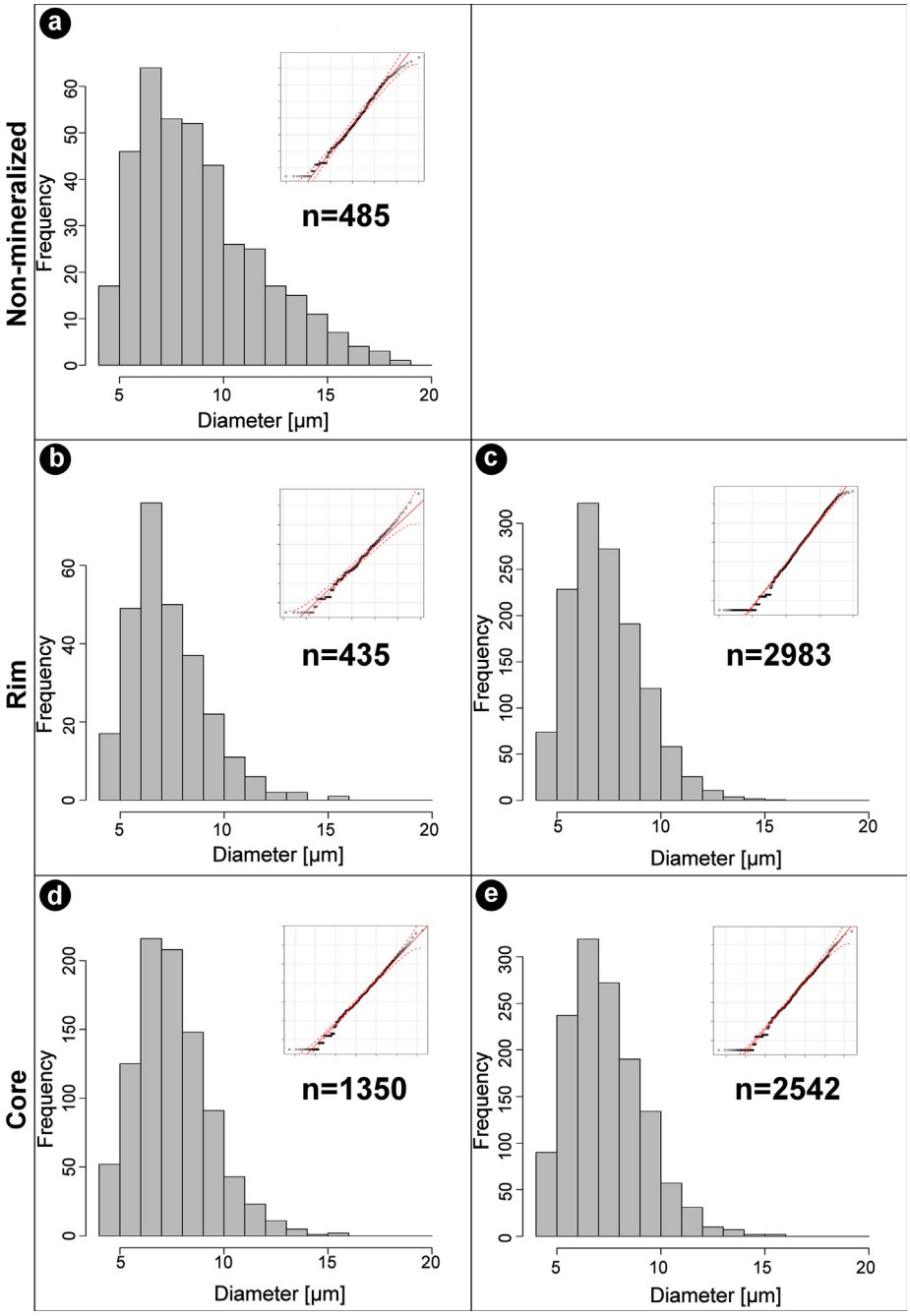

Fig. 5. Absolute frequency histograms of representative populations of framboidal pyrite in non-mineralized limestones, and quantile-quantile plots assessing log-normality, sample NP1 (a); framboidal pyrite and chalcopyrite in limestones from the margins of the orebodies, samples RP1 (b) and RC2 (c), respectively; framboidal pyrite and bornite in limestones from the centre of the orebodies, samples CP1 (d) and CB2 (e), respectively.

The representative size distribution of framboidal pyrite was obtained from three samples: non-mineralized limestone (NP1); mineralized limestone from the margin (RP1); and mineralized limestone from the centre of the orebody (CP1). The representative size distribution of framboidal chalcopyrite was obtained from one sample of mineralized limestone from the margin (RC2), and that of framboidal bornite from one sample of mineralized limestone from centre of the orebody (CB2).

The mean size and the standard deviation of framboidal pyrite in non-mineralized limestone (sample NP1) are 7.77 and 2.12 µm respectively. At the margin of the orebody, the mean size of framboidal pyrite (sample RP1) is 7.25 µm and the standard deviation 1.73 µm. By contrast, the mean size of framboidal chalcopyrite (sample RC2) is 7.35 µm and the standard deviation 1.76 µm. Finally, in the centre of the orebody, the mean size of framboidal pyrite (sample CP1) is 7.50 µm and the standard deviation 1.78 µm, whereas the mean size and the standard deviation of framboidal bornite (sample CB2) are 7.34 and 1.82 µm respectively. Histograms and QQ-plots of each size distribution are shown in Fig. 5. A chi-square test of homogeneity was applied to the frequency counts (size of class = 0.5 µm) of each framboidal size distribution in order to determine if they have similar distributions. The p-value obtained from this chi-square test is 1, the chi-squared statistic is 31.56, and the degrees of freedom are 76, accepting the null hypothesis of homogeneity and therefore concluding that the five populations of framboids are identically distributed.

5. Discussion

Chilean stratabound or manto-type copper deposits mainly occur in Early Upper Jurassic to Late Lower Cretaceous volcano-sedimentary sequences of the Coastal Range of northern and north-central Chile. Kojima et al. (2009) suggest that these deposits were formed epigenetically by the hydrothermal interaction between non-magmatic surface-derived brines and volcano-sedimentary host rocks.

The copper mineralization at the Picachos Project occurs in stratabound manto-type bodies, within the volcano-sedimentary sequence of limestones of the Arqueros Formation, and intercalated with dacitic volcanic rocks. Geographically, the Picachos Project is located in the Coastal Range of north-central Chile, where Kojima et al. (2009) propose the genetic formation model of Chilean manto-type copper deposits. Moreover, the metal zoning of mineralized orebodies of the Picachos Project, with increasing Cu contents from the margin to the centre, is typical for this type of deposits (e.g. Boric et al., 2002; Saric et al., 2003; Oliveros et al., 2008). Hydrothermal alteration of the host rocks in Picachos is especially notable in dacitic volcanic rocks, with replacement of plagioclase by K-feldspar and albite, and subsequent chloritization and sericite alteration. These patterns of sodic and potassic hydrothermal alteration also frequently occur in Chilean manto-type copper deposits (e.g. Boric et al., 2002; Kojima et al., 2003; Cisternas and Hermosilla, 2006; Oliveros et al., 2008). Therefore, and applying the model of Kojima et al. (2009) for Chilean manto-type deposits to the Picachos Project, the host rocks in the Arqueros Formation probably formed prior to copper mineralization. Evidence of this is the replacement of pyrite framboids by chalcopyrite and subsequently by bornite, thereby preserving the framboidal texture (see below), and the preservation of the framboidal texture of pyrite in non-mineralized limestones.

Framboidal pyrite in non-mineralized limestones occurs in close relationship with organic matter and euhedral ankerite (Fig. 3d). This suggests the formation of framboidal pyrite as a consequence of the anaerobic oxidation of the organic matter and the activity of sulphate reducing bacteria (Wilkin and Barnes, 1997; Butler and Rickard, 2000). No overgrowth or sunflower textures developed in this framboidal pyrite; likewise, neither recrystallization nor dissolution signals are observed in the framboids. This indicates the preservation of the original shape of framboidal pyrite in non-mineralized limestones from the Picachos Project (e.g. Ye et al., 2017) and, therefore, the observed size distribution of framboids in sample NP1 is indicative of the redox conditions during limestone formation. The preservation of organic matter in these rocks can delay the oxidation of framboidal pyrite and aid in maintaining the framboids' original shapes (Rigby et al., 2006).

Reported cases of the occurrence of framboidal chalcopyrite are scarce, and its formation is debated (e.g. Oszczepalski, 1999; Wilson and Zentilli, 1999; Hu et al., 2015). Table 2 contains a synopsis of the geological characteristics of these deposits containing framboidal chalcopyrite. Oszczepalski (1999) reports the mimetic replacement of framboidal pyrite by chalcopyrite, bornite and digenite in the Kupferschiefer polymetallic mineralization in Poland. Wilson and Zentilli (1999) also report the replacement of framboidal pyrite formed in stage I of the mineralization by chalcopyrite, bornite and chalcocite during stage II of mineralization in the El Soldado Chilean manto-type deposit. In both cases, the evidence for replacement lies in the presence of remnant pyrite in the framboidal texture of Cu-sulphides. Its genesis is attributed to the alteration of pyrite by cupriferous fluids (Oszczepalski, 1999; Wilson and Zentilli, 1999).

In the studied samples of the Picachos copper Project, no relicts of pyrite are observed in the framboidal texture of chalcopyrite. The lack of significant differences in the mean and standard deviation of sizes, and the chi-square test of homogeneity, indicate that framboids of pyrite and chalcopyrite are identically distributed, suggesting a complete pseudomorphic replacement of pyrite by chalcopyrite, and preserving the shape of primary framboidal pyrite without any evidence of

Table 2
Synopsis of geological characteristics of ore deposits containing framboidal Cu sulphides.

Area	Host rock lithology	Principal deposit	Deposit type	Copper sulphides	Framboidal sulphides	Genesis of chalcopyrite framboids. Evidence	Age (Ma)	Reference
Kupferschiefer (Poland)	Red shales (oxidized facies), reddish-grey shales (transiction facies) and black shales (reduced facies)	Lubin district	Stratabound	Bn, CC and Cp	Py, Cp, Bn and Cc	Replacement of pyrite by chalcopyrite. Remnants of corroded pyrite	256–239	Oszczepalski (1999)
Santiago (Chile)	Bimodal volcanic rocks with marine sediments	El Soldado	Stratabound	Bn, CC and Cp	Py, Cp, Bn and Cc	Replacement of pyrite by chalcopyrite. Remnant pyrite	103 ± 3	Wilson and Zentilli (1999)
Otago Schist (New Zeland)	Syndeformational quartz veins and adjacent sheared and hydrothermally altered schists	Macraes	Gold	Cp	Py and Cp	Analogous processes to those of Oszczepalski (1999). No evidence	–	Hu et al. (2015)

Bn, bornite; Cc, chalcocite-digenite; Cp, chalcopyrite; Py, pyrite.

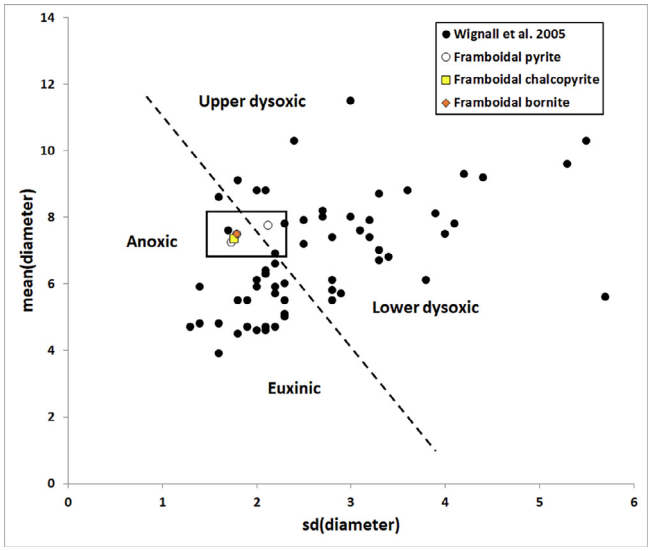

Fig. 6. Standard deviation *vs.* mean diameter of the five representative size distributions of framboids. Framboid populations from Wignall et al. (2005) are plotted for reference. Limits of the redox conditions are from Bond and Wignall (2010).

overgrowths or dissolution. Additional evidence of the replacement of pyrite by chalcopyrite is the geochemical composition of the framboidal chalcopyrite. Framboidal chalcopyrite exhibits a large range of variation in Fe and Cu contents, indicating a geochemical composition ranging from Cu-rich pyrite to stoichiometric chalcopyrite (Table 1).

The origin of framboidal bornite also points to a pseudomorphic replacement of previous framboids. The formation of framboidal bornite is attributed to the replacement of framboidal pyrite by Oszczepalski (1999) and Wilson and Zentilli (1999). Here, no evidence of this process is observed and, therefore, the formation of framboidal bornite from framboidal chalcopyrite cannot be ruled out. Moreover, evidence points to the replacement of chalcopyrite by bornite in the framboidal textures at the centre of the orebodies from the Picachos Project. Framboidal bornite does not show signs of overgrowth or dissolution, indicating the preservation of the shape of the original framboids. Populations of framboidal bornite and chalcopyrite are identically distributed, as indicated in the chi-square test of homogeneity. The formation of bornite at the centre of the orebodies from Picachos is attributed to the pseudomorphic replacement of chalcopyrite or through its growth inside the chalcopyrite grains (Fig. 4d). Zhao et al. (2014) report the replacement of chalcopyrite by bornite under different hydrothermal conditions of solutions containing Cu; however, the formation of bornite directly from pyrite has not been documented.

6. Conclusions

The copper mineralization at the Picachos Project shows typical characteristics of Chilean stratabound or manto-type copper deposits. Such characteristics include: (1) the type of host rocks; (2) the chemical zoning of the orebodies with increasing Cu contents from the margin to the centre; and (3) the sodic and potassic hydrothermal alteration produced by mineralization inside the host rocks.

The preservation of the original framboidal textures of pyrite in non-mineralized and mineralized limestones makes it possible to determine the paleo-redox limestone formation conditions. According to the plots of mean and standard deviation of representative populations of framboidal pyrite in Fig. 6, the Picachos Project limestones were formed under anoxic conditions near the limit of dysoxic conditions. This result is compatible with previous interpretations of the origin of limestones in the Arqueros Formation, and its formation under shallow marine conditions (Aguirre and Egert, 1965; Emparán and Pineda, 2006). Moreover, the size distribution of framboidal chalcopyrite and bornite also indicates the paleo-redox conditions of the limestone formation (Fig. 6). The formation of chalcopyrite by the replacement of primary framboidal pyrite, preserving the framboids' shapes, means that the size distribution of framboidal chalcopyrite is identical to those of the framboidal pyrite. Framboidal bornite is also formed through the pseudomorphic replacement of framboids, thus preserving the original size distribution of framboidal pyrite.

Declaration of Competing Interest

There is no conflict of interest in our work.

Acknowledgements

This paper was made possible by Herencia Resources Plc., which provided access to drill cores and geological information. We would like to thank the technical staff of Herencia Resources Plc. at the Picachos Project for their assistance during our studies. Micro-CT analyses were performed in the Microscopy and Micro-Computed Tomography Laboratory at CENIEH, with the help of CENIEH staff. We would like to thank Belén Notario and Santiago Gil for their assistance at the CENIEH facilities. We also wish to thank Alfredo Larios (ICTS National Centre for Electron Microscopy, Complutense University of Madrid) for his assistance with the photomicrographs. We are also indebted to Nicholas Callaway for his help in reviewing and editing the English of the manuscript. This research was financed by the project CGL2014-53210-P of the Spanish Ministry of Economy and Competitiveness, project PETROSIS PA-18-ACB17-11, granted by the Spanish FCYT and the Government of Asturias, Spain, and the company Herencia Resources Plc. Finally, we thank Franco Pirajno and Daniel Müller, editors of OGR, and three anonymous reviewers whose comments and suggestions have greatly contributed to improving the paper.

Appendix A. Supplementary data

Supplementary data to this article can be found online at https://doi.org/10.1016/j.oregeorev.2019.103037.

References

Aguirre, L., Egert, E., 1965. Cuadrángulo Quebrada Marquesa, Provincia de Coquimbo. Instituto de Investigaciones Geológicas (Chile), escala 1: 50 000, 92.

Bond, D.P.G., Wignall, P.B., 2010. Pyrite framboid study of marine Permian-Triassic boundary sections: a complex anoxic event and its relationship to contemporaneous mass extinction. Geol. Soc. Am. Bull. 122, 1265–1279. https://doi.org/10.1130/B30042.1.

Boric, R., Holmgren, C., Wilson, N.S.F., Zentilli, M., 2002. The geology of the El Soldado Manto type Cu (Ag) deposit, Central Chile. In: In: Porter, T.M. (Ed.), Hydrothermal Iron Oxide Copper-Gold and Related Deposits: A Global Perspective, vol. 2. PGC Publishing, Adelaide, pp. 163–184.

Butler, I.B., Rickard, D., 2000. Framboidal pyrite formation via the oxidation of iron (II) monosulfide by hydrogen sulphides. Geochim. Cosmochim. Acta 64, 2665–2672. https://doi.org/10.1016/S0016-7037(00)00387-2.

Cárdenes, V., Cnudde, V., Merinero, R., Dewanckele, J., De Boever, W., Cnudde, J.P., 2015. Determination of the REDOX paleoconditions: A High Resolution X-ray Tomography study of micro pyrite occurrence. In: Long, B., Francus, P. (Eds.), 2nd International Conference on Tomography of Materials and Structures. INRS, Quebec.

Cárdenes, V., Merinero, R., De Boever, W., Rubio-Ordóñez, Á., Dewanckele, J., Cnudde, J.P., Boone, M., Van Hoorebeke, L., Cnudde, V., 2016. Characterization of micro-pyrite populations in low-grade metamorphic slate: A study using high-resolution X-ray tomography. Palaeogeogr. Palaeoclimatol. Palaeoecol. 441, 924–935. https://doi.org/10.1016/j.palaeo.2015.10.044.

Cárdenes, V., Merinero, R., López-Mungira, A., Rubio-Ordóñez, A., Pitcairn, I.K., Cnudde, V., 2018. Size evolution of micropyrite from diagenesis to low-grade metamorphism. In: Ferrero, S., Lanari, P., Gonçalves, P., Grosch, E.G. (Eds.), Metamorphic Geology: Microscale to Mountain Belts. Geological Society, London, Special Publications, pp. 478.

Carrillo-Rosúa, J., Boyce, A.J., Morales-Ruano, S., Morata, D., Roberts, S., Munizaga, F., Moreno-Rodríguez, V., 2014. Extremely negative and inhomogeneous sulfur isotope signatures in Cretaceous Chilean manto-type Cu–(Ag) deposits, Coastal Range of central Chile. Ore Geol. Rev. 56, 13–24. https://doi.org/10.1016/j.oregeorev.2013.06.013.

Cavalazzi, B., Barbieri, R., Cady, S.L., George, A.D., Gennaro, S., Westall, F., Lui, A., Canteri, R., Rossi, A.P., Ori, G.G., Taj-Eddine, K., 2012. Iron-framboids in the hydrocarbon-related Middle Devonian Hollard Mound of the Anti-Atlas mountain range in Morocco: evidence of potential microbial biosignatures. Sed. Geol. 263–264, 183–193. https://doi.org/10.1016/j.sedgeo.2011.09.007.

Cavalazzi, B., Agangi, A., Barbieri, R., Franchi, F., Gasparotto, G., 2014. The formation of low-temperature sedimentary pyrite and its relationship with biologically-induced processes. Geol. Ore Deposits 56, 395–408. https://doi.org/10.1134/S107570151405002X.

Cisternas, M.E., Hermosilla, J., 2006. The role of bitumen in strata-bound copper deposit formation in the Copiapo area, Northern Chile. Miner. Deposita 41, 339–355. https://doi.org/10.1007/s00126-006-0063-9.

Dallmeyer, D., Brown, M., Grocott, J., Taylor, G., Treloar, P.J., 1996. Mesozoic magmatic and tectonic events within the Andean Plate boundary zone, 26°–27°30'S, North Chile: constraints from $^{40}Ar/^{39}Ar$ mineral ages. J. Geol. 104, 19–40. https://doi.org/10.1086/629799.

Emparán, C., Pineda, G., 2006. Geología del Área Andacollo-Puerto Aldea, Región de Coquimbo. Servicio Nacional de Geología y Minería. Santiago, Carta Geológica de Chile, Serie Geología Básica 96.

Guzmán, J., Collao, S., Oyarzun, R., 2000. Andacollo copper–gold district, La Serena, Chile: preliminary data from the porphyry copper and possible relationships between Cu and Au mineralization. Appl. Earth Sci. 109, 121–125. https://doi.org/10.1179/aes.2000.109.2.121.

Hayes, T.S., Cox, D.P., Piatak, N.M., Seal, R.R.II, 2015. Sediment-hosted stratabound copper deposit model: U.S. Geological Survey Scientific Investigations Report 2010–5070–M, 147 p. https://doi.org/10.3133/sir20105070M.

Hu, S., Evans, K., Craw, D., Rempel, K., Bourdet, J., Dick, J., Grice, K., 2015. Raman characterization of carbonaceous material in the Macraes orogenic gold deposit and metasedimentary host rocks, New Zealand. Ore Geol. Rev. 70, 80–95. https://doi.org/10.1016/j.oregeorev.2015.03.021.

Jarosewich, E., Nelen, J.A., Norberg, J.A., 1980. Reference samples for electron microprobe analysis. Geostandard Newsletter 4, 43–47. https://doi.org/10.1111/j.1751-908X.1980.tb00273.x.

Kojima, S., Astudillo, J., Rojo, J., Tristá, D., Hayashi, K., 2003. Ore mineralogy, fluid inclusion, and stable isotopic characteristics of stratiform copper deposits in the coastal Cordillera of northern Chile. Miner. Deposita 38, 208–216. https://doi.org/10.1007/s00126-002-0304-5.

Kojima, S., Tristá-Aguilera, D., Hayashi, K., 2009. Genetic aspects of the manto-type copper deposits based on geochemical studies of north Chilean deposits. Resour. Geol. 59, 87–98. https://doi.org/10.1111/j.1751-3928.2008.00081.x.

McGuire, A.V., Francis, C.A., Dyar, M.D., 1992. Mineral standards for electron microprobe analysis of oxygen. Am. Mineral. 77, 1087–1091.

Merinero, R., Cárdenes, V., Lunar, R., Boone, M.N., Cnudde, V., 2017. Representative size distributions of framboidal, euhedral, and sunflower pyrite from high-resolution X-ray tomography and scanning electron microscopy analyses. Am. Mineral. 102, 620–631. https://doi.org/10.2138/am-2017-5851.

Oliveros, V., Féraud, G., Aguirre, L., Fornari, M., 2006. The Early Andean Magmatic Province (EAMP): $^{40}Ar/^{39}Ar$ dating on Mesozoic volcanic and plutonic rocks from the Coastal Cordillera, northern Chile. J. Volcanol. Geoth. Res. 157, 311–330. https://doi.org/10.1016/j.jvolgeores.2006.04.007.

Oliveros, V., Tristá-Aguilera, D., Féraud, G., Morata, D., Aguirre, L., Kojima, S., Ferraris, F., 2008. Time relationships between volcanism–plutonism–alteration–mineralization in Cu-stratabound ore deposits from the Michilla mining district, northern Chile: a $^{40}Ar/^{39}Ar$ geochronological approach. Miner. Deposita 43, 61–78. https://doi.org/10.1007/s00126-007-0147-1.

Ollion, J., Cochennec, J., Loll, F., Escudé, C., Boudier, T., 2013. TANGO: a generic tool for high-throughput 3D image analysis for studying nuclear organization. Bioinformatics 29, 1840–1841. https://doi.org/10.1093/bioinformatics/btt276.

Oszczepalski, S., 1999. Origin of the Kupferschiefer polymetallic mineralization in Poland. Miner. Deposita 34, 599–613. https://doi.org/10.1007/s001260050222.

Peckmann, J., Thiel, V., 2004. Carbon cycling at ancient methane–seeps. Chem. Geol. 205, 443–467. https://doi.org/10.1016/j.chemgeo.2003.12.025.

Pichowiak, S., 1994. Early Jurassic to Early Cretaceous magmatism in the Coastal Cordillera and the Central Depression of North Chile. In: Reutter, K.J., Scheuber, E., Wigger, P.J. (Eds.), Tectonics of the Southern Central Andes. Springer-Verlag, Stuttgart, Structure and evolution of a Continental Margin, pp. 203–217.

R_Core_Team, 2017. R: A language and environment for statistical computing, https://www.R-project.org/. R Foundation for Statistical Computing, Vienna.

Rajabpour, S., Abedini, A., Alipour, S., Lehmann, B., Jiang, S.Y., 2017. Geology and geochemistry of the sediment-hosted Cheshmeh-Konan redbed-type copper deposit, NW Iran. Ore Geol. Rev. 86, 154–171. https://doi.org/10.1016/j.oregeorev.2017.02.013.

Reyes, M., 1991. The Andacollo strata-bound gold deposit, Chile, and its position in a porphyry copper-gold system. Econ. Geol. 86, 1301–1316. https://doi.org/10.2113/gsecongeo.86.6.1301.

Rickard, D., 2019. Sedimentary pyrite framboid size-frequency distributions: a meta-analysis. Palaeogeogr. Palaeoclimatol. Palaeoecol. 522, 62–75. https://doi.org/10.1016/j.palaeo.2019.03.010.

Rigby, P.A., Dobos, S.K., Cook, F.J., Goonetilleke, A., 2006. Role of organic matter in framboidal pyrite oxidation. Sci. Total Environ. 367, 847–854. https://doi.org/10.1016/j.scitotenv.2004.10.011.

Royston, P., 1995. Remark AS R94: A remark on Algorithm AS 181: The W test for normality. Appl. Stat. 44, 547–551.

Sadati, S.N., Yazdi, M., Mao, J., Behzadi, M., Adabi, M.H., Lingang, X., Zhenyu, C., Mokhtari, M.A.A., 2016. Sulfide mineral chemistry investigation of sediment-hosted stratiform copper deposits, Nahand-Ivand area, NW Iran. Ore Geol. Rev. 72, 760–776. https://doi.org/10.1016/j.oregeorev.2015.09.018.

Saric, N., Kreft, C., Huete, C., 2003. Geología del yacimiento Lo Aguirre, Chile. Revista Geológica de Chile 30, 317–331. https://doi.org/10.4067/S0716-02082003000200010.

Schindelin, J., Arganda-Carreras, I., Frise, E., Kaynig, V., Longair, M., Pietzsch, T., Preibisch, S., Rueden, C., Saalfeld, S., Schmid, B., Tinevez, J.Y., White, D.J., Hartenstein, V., Eliceiri, K., Tomancak, P., Cardona, A., 2012. Fiji: an open-source platform for biological-image analysis. Nat. Methods 9, 676–682.

Schoonen, M.A.A., 2004. Mechanisms of sedimentary pyrite formation. In Amend, J.P., Edwards, K.J., Lyons, T.W. (Eds.) Sulfur biogeochemistry—Past and present: Boulder, Colorado, Geological Society of America Special Paper 379: 117–134.

Scott, R.J., Meffre, S., Woodhead, J., Gilbert, S.E., Berry, R.F., Emsbo, P., 2009. Development of framboidal pyrite during diagenesis, low-grade regional metamorphism, and hydrothermal alteration. Econ. Geol. 104, 1143–1168. https://doi.org/10.2113/gsecongeo.104.8.1143.

Scrucca, L., Fop, M., Murphy, T.B., Raftery, A.E., 2016. mclust 5: clustering, classification and density estimation using Gaussian finite mixture models. The R Journal 8, 289–317.

Tian, L., Tong, J.N., Algeo, T.J., Song, H.J., Song, H.Y., Chu, D.L., Shi, L., Bottjer, D.J., 2014. Reconstruction of Early Triassic ocean redox conditions based on framboidal pyrite from the Nanpanjiang Basin, South China. Palaeogeogr. Palaeoclimatol. Palaeoecol. 412, 68–79. https://doi.org/10.1016/j.palaeo.2014.07.018.

Wang, P., Huang, Y., Wang, C., Feng, Z., Huang, Q., 2012. Pyrite morphology in the first member of the Late Cretaceous Qingshankou Formation, Songliao Basin, Northeast China. Palaeogeogr. Palaeoclimatol. Palaeoecol. 385, 125–136. https://doi.org/10.1016/j.palaeo.2012.09.027.

Wignall, P.B., Newton, R., 1998. Pyrite framboid diameter as a measure of oxygen deficiency in ancient mudrocks. Am. J. Sci. 298, 537–552. https://doi.org/10.2475/ajs.298.7.537.

Wignall, P.B., Newton, R., Brookfield, M.E., 2005. Pyrite framboid evidence for oxygen-poor deposition during the Permian-Triassic crisis in Kashmir. Palaeogeogr. Palaeoclimatol. Palaeoecol. 216, 183–188. https://doi.org/10.1016/j.palaeo.2004.10.009.

Wilkin, R.T., Barnes, H.L., Brantley, S.L., 1996. The size distribution of framboidal pyrite in modern sediments: An indicator of redox conditions. Geochim. Cosmochim. Acta 60, 3897–3912. https://doi.org/10.1016/0016-7037(96)00209-8.

Wilkin, R.T., Barnes, H.L., 1997. Formation processes of framboidal pyrite. Geochim. Cosmochim. Acta 61, 323–339. https://doi.org/10.1016/S0016-7037(96)00320-1.

Wilson, N.F.S., Zentilli, M., 1999. The role of organic matter in the genesis of the El Soldado volcanic-hosted manto-type Cu deposit, Chile. Econ. Geol. 94, 1115–1136. https://doi.org/10.2113/gsecongeo.94.7.1115.

Xiao, Y.F., Wu, K., Tian, L., Benton, M.J., Du, Y., Yang, H., Tong, J.N., 2018. Framboidal pyrite evidence for persistent low oxygen levels in shallow-marine facies of the Nanpanjiang Basin during the Permian-Triassic transition. Palaeogeogr. Palaeoclimatol. Palaeoecol. 511, 243–255. https://doi.org/10.1016/j.palaeo.2018.08.012.

Ye, Y., Wu, C., Zhai, L., An, Z., 2017. Pyrite morphology and episodic euxinia of the Ediacaran Doushantuo Formation in South China. Sci. China Earth Sci. 60, 102–113. https://doi.org/10.1007/s11430-016-0066-0.

Zhao, J., Brugger, J., Ngothai, Y., Pring, A., 2014. The replacement of chalcopyrite by bornite under hydrothermal conditions. Am. Mineral. 99, 2389–2397. https://doi.org/10.2138/am-2014-4825.